Open Access
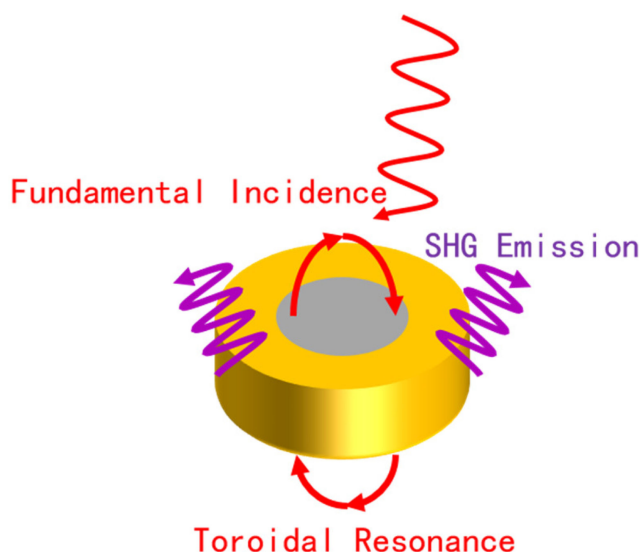
Second Harmonic Generation Enhancement From Plasmonic Toroidal Resonance in Core-Shell Nanodisk

Kai Guo
Keya Zhou
Wei Liu
Zhongyi Guo

Second Harmonic Generation Enhancement From Plasmonic Toroidal Resonance in Core-Shell Nanodisk

Kai Guo ,[1,4] **Keya Zhou,**[2] **Wei Liu,**[3] **and Zhongyi Guo** [1]

[1]School of Computer Science and Information Engineering, Hefei University of Technology,
Hefei 230601, China
[2]School of Physics, Harbin Institute of Technology, Harbin 150001, China
[3]School of Electronic and Information Engineering, Harbin Institute of Technology,
Shenzhen 518055, China
[4]State Key Laboratory of Millimeter Waves, Southeast University, Nanjing 210096, China

Abstract: Toroidal multipoles, together with electric and magnetic multipoles, provide a complete description of electromagnetic responses of matter. The fundamental toroidal resonance has been extensively achieved and investigated in nanooptics, showing great ability to increase light absorption and light force. In this paper, we obtained plasmonic toroidal dipole resonance in core-shell (dielectric-core/gold-shell) nanodisk and demonstrated an enhanced second harmonic generation (SHG) from this resonance. It was shown that the toroidal dipole resonance based SHG depends on the refractive index of dielectric-core. For large refractive index cases, head-to-tail magnetic dipole pairs form a close loop, which is a signature of toroidal dipole and results in the enhancement of SHG. In addition, the frequency of this SHG red shifts as the refractive index of dielectric-core increases. We also investigated the cases in which the dielectric-core is filled with several common materials. Moreover, the toroidal resonance based SHG depends on both inner and outer radius of the core-shell nanodisk. Such results may serve for the developments of nonlinear nanooptics and their applications.

Index Terms: Plasmonic toroidal resonance, second harmonic generation, metamolecule.

1. Introduction

Second harmonic generation (SHG) from nanostructures is at the heart of metamaterials and nanooptics since it does not strictly require the macroscale phase-matching condition [1, 2]. Especially, the miniaturization and integration trends of metamaterials make it possible to engineer and utilize SHG in many applications, such as characterizations of structural properties and laser beam [1]. In the past decades, plasmonics have been a hot research field owing to their unique ability to concentrate light in nanoscale volume much smaller than the diffraction limit [3]. Therefore, one of the goals for practical application of SHG from plasmonic nanostructures is to make full use of near-field enhancement of light, achieving high efficiency of SHG. In this regard, various methods have been designed to concentrate light in a small size and obtain efficiently conversion

of fundamental incidence into emissions with double-frequency [4]–[9]. For this purpose, a direct approach to enhance SHG is exploiting electric and magnetic multipoles, which could significantly increase localized surface plasmon resonances and near-field intensity [10]–[15].

As the third set of electromagnetic multipoles, toroidal type resonances, together with electric and magnetic multipoles, could fully describe electromagnetic responses of matter [16]–[18]. It is well known that the electric and magnetic multipoles correspond to charge oscillations and current-loops, respectively. In contrast, toroidal multipoles correspond to oscillating radial currents. However, toroidal multipoles are usually less known owing to their relative weakness compared with the electric and magnetic counterparts. In 2007, a 3D-array of toroidal solenoids was designed to produce toroidal response which can be easily observed in experiment [19]. It was shown that the toroidal dipole can be viewed as a set of magnetic dipoles with head-to-tail arrangement along a loop. Thereafter, the fundamental toroidal multipoles, *i.e.*, toroidal dipole resonances, have been achieved in both 2D and 3D architectures from visible to terahertz regions [20]–[27]. In addition, toroidal dipole resonance based metamaterials opened a new route to many exciting applications, such as optical force enhancement [28], sensing [29], light absorption [30], transparency [31], unidirectional scattering [32], and even enhanced nonlinear emissions [33]. These applications take the unique advantage of toroidal dipole resonance in squeezing electromagnetic field and high-quality values. In this sense, the toroidal dipole resonance could be a great candidate for boosting second harmonic generation from a plasmonic nanostructure.

In this paper, we design a dielectric-core/gold-shell plasmonic nanodisk to achieve toroidal dipole resonance based SHG enhancement. Numerical simulations are performed to investigate the optical responses of the designed nanostructure in both linear and nonlinear processes. The near-field distributions of electric and magnetic components in linear process are plotted to demonstrate the emergence of toroidal dipole resonance. On this basis, the dependence of SHG on refractive index of dielectric core are studied. To make these results more practical, we compare the SHG efficiency and wavelength when the dielectric core is filled with typical materials. Additionally, the SHG emission from the designed nanostructure with different inner and outer radius are shown. These results may promote the practical application of both toroidal dipole resonance and nonlinear nanooptics.

2. Results and Discussion

Fig. 1(a) schematically shows the designed dielectric-core/gold-shell nanodisk which may support toroidal dipole resonance. For simplicity, we assumed the plasmonic nanodisk is free-standing and the surrounding medium is air. To achieve emergence of toroidal dipole resonance, the dielectric-core should be with high refractive index [30]. For comparison, we also calculated the linear optical responses of gold-shell and dielectric-core, as schematically shown in Figs. 1(b) and 1(c), respectively. In these cases, the refractive index of dielectric-core is $n = 3.0$. The inner and outer radius are $R_1 = 50$ nm and $R_2 = 100$ nm, respectively. The thickness is $t = 100$ nm. A y-polarized plane wave was used as incident source.

Figs 1(d), 1(e) and 1(f) plot the absorption spectrum of the structures in Figs. 1(a), 1(b) and 1(c), respectively, as a function of fundamental wavelength and in-plane wave-vector. The absorption is calculated by 1-T-R, where T and R denote transmission and reflection, respectively. For the dielectric core with $n = 3.0$, no any resonance peak can be observed in the absorption spectrum, it is because the imaginary part of refractive index of dielectric core is zero, as shown in Fig. 1(f). The resonance moves to long wavelength when the in-plane wave-vector increases. For the gold-shell, a broadband absorption peak exists in the short wavelength range and a sharp dropping of absorption can be seen, as shown in Fig. 1(e). When the in-plane wave-vector increases, the wavelength at which the absorption dropping happens also moves to long wavelength. When the dielectric-core integrates with the gold-shell, forming a core/shell nanodisk, the absorption pattern becomes obviously different from those of dielectric-core, gold-shell and their summation, as shown in Fig. 1(b). Besides the broadband absorption peak in the short wavelength range, a narrowband absorption peak arises in the long wavelength range around $\lambda = 850$ nm. Evidently, this new
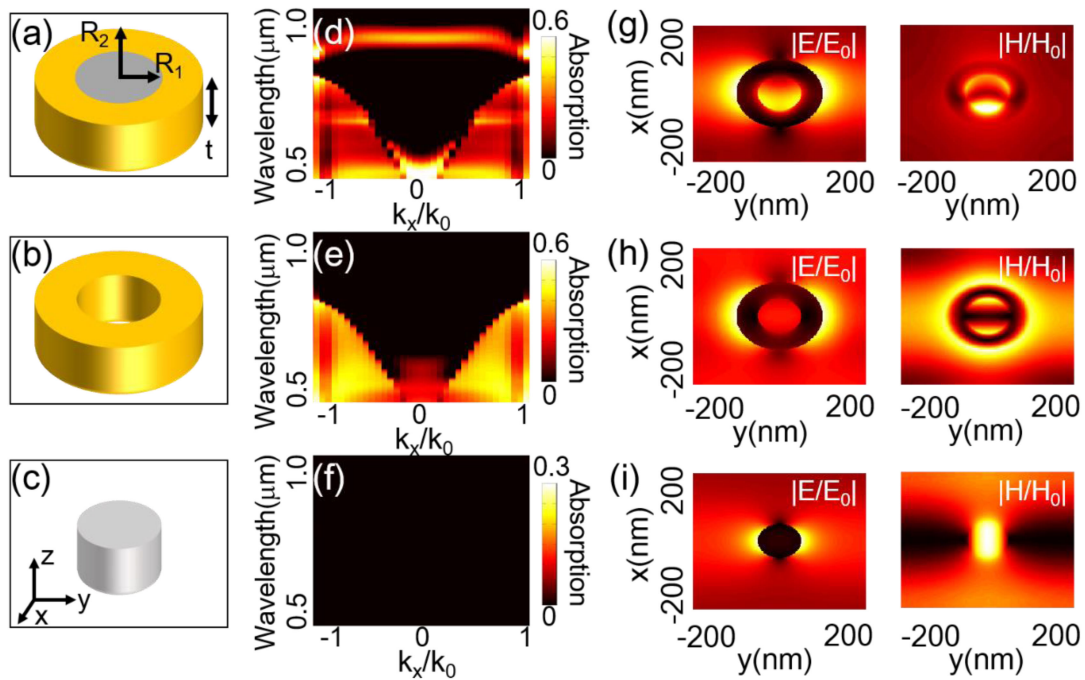
Fig. 1. Emergence of toroidal dipole resonance in a dielectric-core/gold-shell nanodisk. (a) The schematic of designed plasmonic nanodisk. R_1 and R_2 denote the inner and outer radius, respectively, t denotes the thickness. (b) and (c) schematically show the gold-shell and dielectric-core, respectively. (d), (e), and (f) plot the absorption spectra of the structure (a), (b), and (c), respectively, as functions of wavelength and in-plane wave-vector. (g), (h), and (i) show near-field distributions of electric and magnetic components when the in-plane wave-vector $k_x = \sqrt{2}k_0/2$ at wavelength of $\lambda = 710$ nm.

absorption peak may not come from hybridization of the resonances in dielectric-core and gold-shell. It is also worth to note that the new absorption peak is not sensitive to the value of in-plane wave-vector.

To unveil the physical nature of the formation of dielectric-core/gold-shell nanodisk, we plotted the x-y plane near-field distributions of both electric and magnetic components in these three architectures at wavelength of $\lambda = 710$ nm, which is close to both the absorption dropping in Figs. 1(d), 1(e). The in-plane wave-vector is $k_x = \sqrt{2}k_0/2$. For the dielectric-core, a dipolar electric resonance along y-direction and a magnetic hot-spot can be observed, as shown in Fig. 1(i). In addition, a significant amount of both electric and magnetic fields exists in the region between dielectric-core in x-direction, which is the characteristic of an in-plane collective surface mode [34]. For the gold-shell results in Fig. 1(h), the electric field is highly localized at the outer surface, presenting a dipolar electric resonance along y-direction. Although a pair of magnetic resonance existing in the inner core of gold-shell, we may not consider it as a toroidal dipole. It is because the electric component does not significantly concentrate in the inner core. Meanwhile, similarly to the dielectric-core case, both electric and magnetic fields are significantly amplified between the gold-core, showing the existence of in-plane collective surface mode. When the dielectric-core/gold-shell nanodisk is composed, the features of both electric and magnetic field distributions are similar with those of gold-shell. Nevertheless, we need to pay attention to that more electric field is squeezed in the inner core of gold-shell, which may be attributed to toroidal dipole resonance induced by the high charge density in the dielectric-core.

To show the electromagnetic mode evolvement and demonstrate the emergence of toroidal dipole resonance, the normalized electric intensity and magnetic z-component of the dielectric-core/gold-shell nanodisk were plotted at wavelength of $\lambda = 850$ nm, $\lambda = 600$ nm, and $\lambda = 530$ nm, as shown in Fig. 2. The white arrows denote the direction of electric field and the white cross
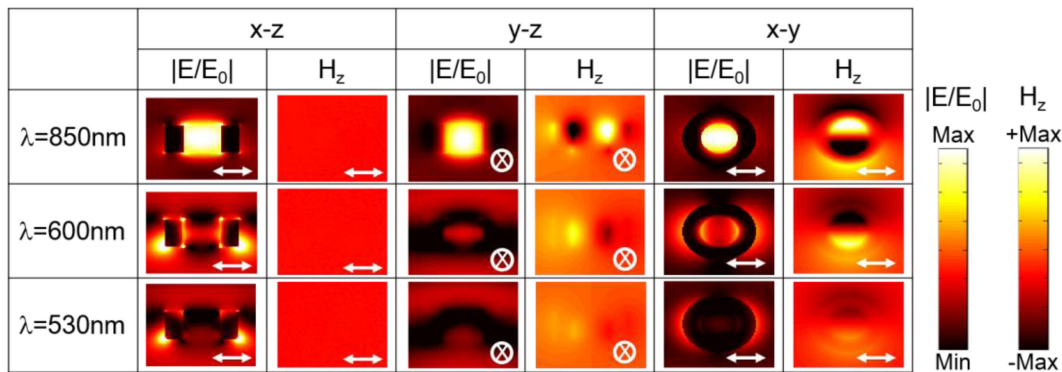
Fig. 2. Near-field distributions of both normalized electric intensity and magnetic *z*-components in the dielectric-core/gold-shell nanodisk under normal incidence. The top, middle, and bottom panels correspond to fundamental wavelength of $\lambda = 850$ nm, $\lambda = 600$ nm, and $\lambda = 530$ nm, respectively. The results in *x-z*, *y-z*, and *y-z* planes are plotted from left to right columns. The white arrows and cross indicate the direction of electric field in each plane. In these results, the refractive index of dielectric-core is $n = 3.0$.

indicates the electric field is perpendicular to y-z plane. When $\lambda = 530$ nm, the electric field is mainly localized at the outer surface of gold-shell, showing an electric dipolar resonance characteristic. When $\lambda = 600$ nm, part of the energy of electric field transfers to the inner surface of gold-shell and an electric dipolar resonance appears. We labeled the electric dipolar resonance at outer and inner surfaces of gold-shell as ED_1 and ED_2, respectively. As the incident wavelength keeps increasing, more energy will transfer to the inner part of gold-shell and be concentrated in the dielectric-core. More importantly, a pair of magnetic dipoles with opposite signs forms a head-to-tail configuration and creates a close-loop of magnetic field [18], which is perpendicular to the direction of electric field and the key feature of toroidal dipole. The simulated results at wavelength of $\lambda = 850$ nm show that the typical features of toroidal dipolar resonance. From the electric field distributions at wavelength of $\lambda = 850$ nm, the energy is also significantly enlarged at the surface of gold-shell, which may give rise to enhanced surface currents with both linear and nonlinear behaviors. One may notice that the head-to-tail magnetic dipole also forms at wavelength of $\lambda = 600$ nm. However, the magnetic field is obviously radiative and leaks to the outer surface of gold-shell. Moreover, the electric intensity is much stronger at the surface of gold-shell than in the dielectric-core. Therefore, we may attribute it to electric dipole rather than toroidal dipole.

As previously discussed, the emergence of toroidal dipole in this structure requires dielectric-core with high refractive index. In addition, the above results inspired us to enhance the SHG emission from the toroidal dipole resonance in dielectric-core/gold-shell nanodisk. To demonstrate, we investigated the dependence of SHG efficiency on the refractive index of dielectric-core and second harmonic wavelength. The SHG efficiency is defined as $\eta^{SHG} = I^{2\omega}/I^{\omega}$, where $I^{2\omega}$ and I^{ω} represent the intensity of scattering field in second harmonic and fundamental process, respectively. The calculated SHG efficiency η^{SHG} is plotted in Fig. 3(a) and there are three bands arising in the pattern (marked by the white dashed lines), corresponding to the ED_1, ED_2, and toroidal dipole resonances. The enhanced SHG efficiency from toroidal dipole emerges when the refractive index of dielectric-core is around $n = 2.0$. As the value of n continues increases, the second harmonic (SH) wavelength red shifts, accompanied by boosting the SHG efficiency. It could be attributed to the increased ability of dielectric-core to concentrate light caused by its high charge density. Additionally, the SHG efficiency from toroidal dipole resonance is much stronger than those from ED_1 and ED_2 for a given refractive index of dielectric-core, demonstrating the light-trapping capability of toroidal dipole resonance and the resulted SHG enhancement.

To further validate the origins of the enhancement of SHG efficiency, the near- and far-field distributions of the SHG electric component were plotted at the fundamental ED_1, ED_2 and toroidal
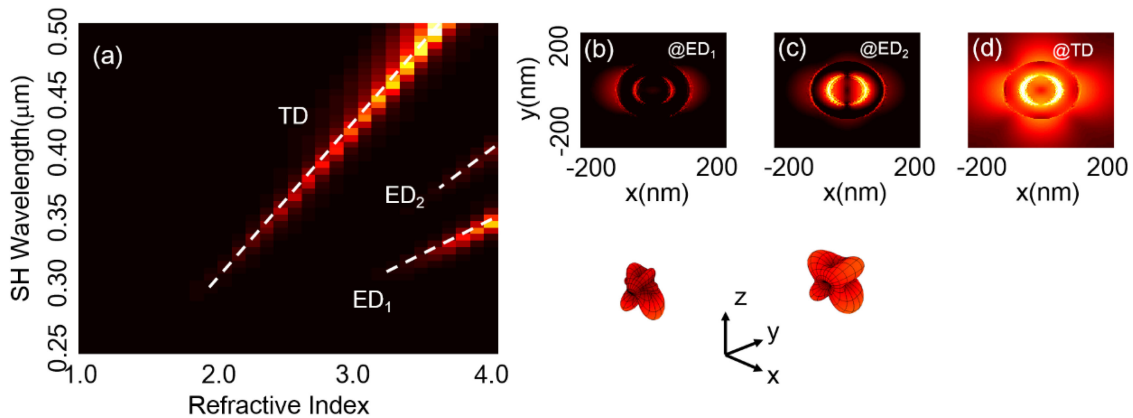
Fig. 3. SHG enhancement induced by toroidal dipole (TD) resonance. (a) The SHG efficiency as a function of both refractive index of dielectric-core and second harmonic (SH) wavelength. ED_1 and ED_2 indicate electric dipole resonances of gold-shell and dielectric-core, respectively. Near- and far-field distributions of SHG electric component at (b) ED_1, (c) ED_2 and (d) TD are shown in the top and bottom panels, respectively. In (b)-(d), the refractive index of dielectric-core is $n = 3.0$.

dipole (TD) resonances, as shown in Figs. 3(b), 3(c) and 3(d), respectively. In these results, the refractive index of dielectric-core is $n = 3.0$. The top panel of Fig. 3(b) presents that the SHG electric field is mainly localized at the two ends of outer surface of gold-shell along x-axis. In contrast, the top panel of Fig. 3(c) presents that the SHG electric field is mainly localized at the two ends of inner surface of gold-shell along x-aixs. These results are in good agreements with the fact that they arise from fundamental ED_1 and ED_2. The near-field pattern of electric field at toroidal dipole (TD) resonance (top panel of Fig. 3(d)) exhibits strong enhancement with a quadrupolar feature at the inner surface of gold-shell. The corresponding far-field distributions in the bottom panel show that the SHG resulted from toroidal dipole (TD) resonance can radiates more energy to far-field. Besides, the SHG radiation patterns of ED_1 and ED_2 differ from that of toroidal dipole (TD), indicating the opportunity to orient the SHG emissions via interference between electromagnetic multipoles and toroidal type resonances. For instance, when the refractive index of dielectric-core is n = 3.0, the SHG efficiency from toroidal dipole resonance is enhanced by a factor of more than 40, relative to those from ED1 and ED2. Considering the simple structure and comparable enhancement of SHG, the designed plasmonic toroidal dipole resonance has unique advantages over the previously reported plasmonic resonances induced SHG [1].

To extend practicality of the proposed method, we investigated the toroidal dipole based SHG emission when the dielectric-core is filled with common materials, including GaN, diamond, Si, TiO_2 and Si_3N_4. The optical constants of these dielectric materials used in simulation were taken from the experiment data [37]. The simulated results of SHG efficiency and SH wavelength are summarized in Table 1. It can be easily seen that these results identify with the dependence of SHG emission on the refractive index of dielectric-core.

It is known that the SHG emission strongly depends on the performance of linear polarization P_1 at the surface of nanostructure, which is sensitive to the geometry parameters. Thus, we investigated the influences of both inner radius (R_1) and outer radius (R_2) on the SHG emission from toroidal dipole resonance. When we changed the value of inner (outer) radius, the outer (inner) radius was a constant of $R_2 = 100$ nm ($R_1 = 50$ nm). In the simulations, the refractive index of dielectric-core was $n = 2.5$. The SHG emissions, including the emitted efficiency and wavelength, as functions of inner radius (R_1) and outer radius (R_2) are plotted in Figs. 4(a) and 4(b), respectively. The insets in Fig. 4(a)(Fig. 4(b)) present the fundamental near-field magnetic intensity in x-y plane when $R_1 = 30$ nm, 55 nm, and 80 nm ($R_2 = 80$ nm, 110 nm, and 120 nm).

As the inner radius R_1 increases from 30 nm to 80 nm, the emitted second harmonic (SH) wavelength monotonously shifts from 325 nm to 490 nm, as shown in Fig. 4(a). It is because

TABLE 1
SHG Emission of the Cases with Different Dielectric-Core

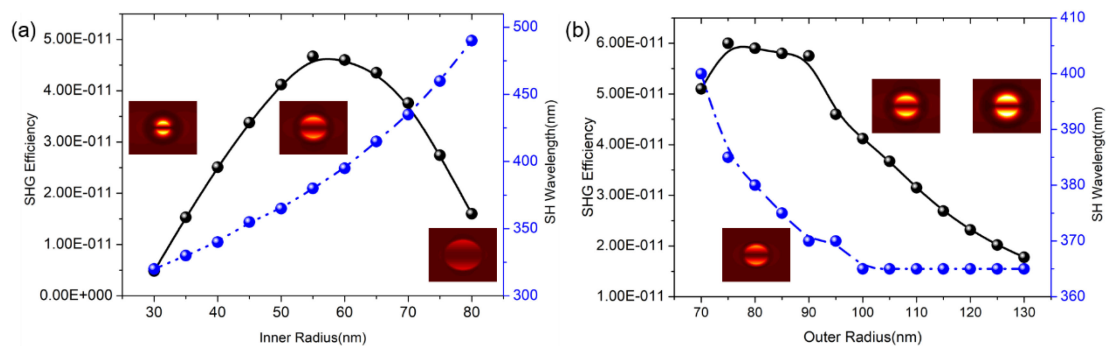|	SHG Efficiency	SH Wavelength
GaN	3.16×10^{-12}	350 nm
Diamond	3.61×10^{-12}	355 nm
Si	1.69×10^{-11}	515 nm
TiO_2	4.55×10^{-12}	370 nm
Si_3N_4	0.96×10^{-12}	315 nm

Fig. 4. Dependences of SHG emission on the (a) inner and (b) outer radius of the proposed dielectric-core/gold-shell nanodisk. The refractive index of dielectric-core is $n = 2.5$. When the inner (outer) radius varies, the outer (inner) radius is $R_2 = 100$ nm ($R_1 = 50$ nm). The insets in (a) ((b)) present the fundamental near-field magnetic intensity in x-y plane when $R_1 = 30$ nm, 55 nm, and 80 nm ($R_2 = 80$ nm, 110 nm, and 120 nm).

toroidal dipole in our proposed method is formed by a pair of head-to-tail magnetic dipoles, which are originated from circular loops of current. When the inner radius R_1 increases, the dielectric-core could support circular loops of current with larger circumference, corresponding to magnetic hot spots with bigger size and incident excitation with longer wavelength (see the insets). As a result, the emitted wavelength of SHG from toroidal dipole resonance monotonously increases with the inner radius R_1. Meanwhile, the SHG efficiency varies with the inner radius R_1 and reaches maximum value around $R_1 = 55$ nm. These phenomena could also be attributed to the physical nature of toroidal dipole resonance. When the inner radius R_1 increases from 30 nm to 55 nm, more energy could be concentrated by the toroidal dipole resonance, resulting in increased SHG efficiency. When the inner radius R_1 increases further, the energy density at toroidal dipole resonance decreases (see the inset at $R_1 = 80$ nm). Consequently, few energies of fundamental incidence could be conversed to SHG emission through the induced nonlinear surface currents.

As the outer radius R_2 increases from 70 nm to 100 nm, the emitted second harmonic (SH) wavelength monotonously shifts from 400 nm to 365 nm, as shown in Fig. 4(b). It could be attributed to the increased inductance of gold-shell, leading to the blue shifts of fundamental toroidal dipole resonance. When the value of R_2 is larger than 100 nm, the SH wavelength shows no significant dependence on R_2 because the gold-shell is thick enough to separate the localized electric field at the outer surface of gold-shell and the dielectric-core. In addition, the radius of dielectric-core is fixed, determining the size of hot magnetic spots (see insets in Fig. 4(b)). Meanwhile, the SHG

TABLE 2
SHG Enhancement in Several Different Mechanism

	Enhancement Factor	Mechanism	Other Requirement
[5]	~5	Electric Dipole	Array
[6]	~35	Electric Fano	Grating
[7]	~30	Electric Fano	Vectorial Beam
[11]	N.A.	Magnetic Fano	Hetero-trimer
[12]	N.A.	Electric Dipole	Nanorod
[13]	~2	Hybridization	Hollow Nanoprism
[14]	N.A.	Electric Fano	Hetero-dimer
[15]	~10	Magnetic Fano	Bianisotropy
This Work	~40	Toroidal Dipole	None

efficiency decreases when the gold-shell becomes thicker, thereby resulting in higher Ohmic loss and reduced SHG emission.

Table 2 summarizes several reported results about SHG enhancement from different mechanisms. It can be seen that our proposed method may have a high enhanced SHG emission from toroidal dipole resonance compared with the other cases. In addition, the proposed method requires no further condition, such as complex structure and excitation beam. More importantly, the toroidal dipole resulted SHG is usually negligible in plamonic structure (about one percent of those from electric and magnetic components). Therefore, the proposed mechanism has the unique advantages over the previously reported results.

3. Conclusion

We designed a core-shell (dielectric-core/gold-shell) nanodisk to achieve toroidal dipole resonance with highly localized electric field intensity. Numerical simulation analysis demonstrated that the toroidal dipole resonance emerges when refractive index of dielectric-core is larger than $n = 2.0$. The key feature of toroidal dipole resonance is that head-to-tail magnetic dipole pairs form a close loop, resulting in the enhancement of SHG. Further investigation showed the frequency of this SHG red shifts when the refractive index of dielectric-core increases. To make the results more practical, we compared the SHG emissions of the cases in which the dielectric-core is filled with GaN, diamond, Si, TiO_2, and Si_3N_4. Finally, it was shown that the toroidal resonance based SHG is sensitive to both inner and outer radius of the core-shell nanodisk. Such results may serve for the developments of toroidal resonances and nonlinear nanooptics.

Simulation Details

Both the linear and nonlinear processes were calculated by using a self-built program based on finite-element-method. Following the reported results, the numerical simulation are two steps [35]. In the first step, the absorption and scattering spectra in linear process were calculated. Period boundaries were adopted in both x- and y-directions to avoid unphysical reflections from boundaries and save simulation memory. Perfect matching layer (PML) were used in z-direction to mimic an open space. In the second step, second harmonic scattering process was simulated with all boundaries were set as PML.

The SHG effect is described by a nonlinear current sheet at the surface of gold. The source of SHG can be expressed as

$$\mathbf{J}_{NL} = \frac{i\omega}{n_0 e}\left[\hat{\mathbf{t}}\left(P_1^{\perp} P_1^{\parallel}\right) + \hat{\mathbf{n}}\frac{1}{2}\frac{3\omega + i\gamma}{2\omega + i\gamma}\left(P_1^{\perp}\right)^2\right] \tag{1}$$

where $\hat{\mathbf{t}}$ and $\hat{\mathbf{n}}$ represent the tangential and normal unit vectors at the surfaces, respectively. $P_1^{\parallel} = \hat{\mathbf{t}} \cdot \mathbf{P}_1$ and $P_1^{\perp} = \hat{\mathbf{n}} \cdot \mathbf{P}_1$, where $\mathbf{P}_1$ is the linear polarization. According to the hydrodynamic model, the nonlinear response includes nonlinear Coulomb term, magnetic Lorentz force contribution, convective terms, and nonlinear pressure term [36]. Among them, the Coulomb term, the pressure term, and part of the convective terms can be clarified as purely surface terms, while the magnetic Lorentz force is purely bulk term, besides, the other part of the convective term contains both surface and bulk contributions. Nevertheless, both theory and experiment have demonstrated that these bulk SHG emissions are usually weak-contributions and could be approximately neglected [1], [35], [36], thus Eq. 1 was used to simulate SHG effect. In the simulations, the optical constants of gold and several typical dielectrics were taken from previously reported results [36]–[38].

It also should be noted that the aforementioned methods to calculate SHG is for simplifying the simulations but reasonable in our case. On the one hand, we are focusing on nonlinearity caused by plasmonic effects, in which the electromagnetic fields are highly localized at and evanescent from the surface of plasmonic structure. On the other hand, it is convenient for simulation due to lacking of nonlinear response of dielectric-core with arbitrary refractive index. Nevertheless, even if we considered the second harmonic generation from several typical dielectric material, e.g., Si, there is no significant influence on the enhancement of SHG induced by toroidal dipole.

References

[1] J. Butet, P. F. Brevet, and O. J. F. Martin, "Optical second harmonic generation in plasmonic nanostructures: From fundamental principles to advanced applications," *ACS Nano*, vol. 9, no. 11, pp. 10545–10562, 2015.

[2] R. Savo *et al.*, "Broadband mie driven random quasi-phase-matching," *Nat. Photon.*, vol. 14, pp. 740–747, 2020.

[3] H. Fischer and O. J. F. Martin, "Engineering the optical response of plasmonic nanoantennas," *Opt. Exp.*, vol. 16, no. 12, pp. 9144–9154, 2008.

[4] S. A. Scherbak and A. A. Lipovskii, "Understanding the second harmonic generation enhancement and behavior in metal core-dielectric shell nanoparticles," *J. Phys. Chem. C*, vol. 122, no. 27, pp. 15635–15645, 2018.

[5] R. Czaplicki *et al.*, "Less is more: Enhancement of second-harmonic generation from metasurfaces by reduced nanoparticle density," *Nano Lett.*, vol. 18, pp. 7709–7714, 2018.

[6] H. H. Hsiao *et al.*, "Enhancement of second-harmonic generation in nonlinear nanolaminate metamaterials by nanophotonic resonances," *Opt. Exp.*, vol. 24, no. 9, pp. 9651–9659, 2016.

[7] W. Shang, F. Xiao, L. Han, M. Premaratne, T. Mei, and J. Zhao, "Enhanced second harmonic generation from a plasmonic fano structure subjected to an azimuthally polarized light beam," *J. Phys.: Condens. Matter.*, vol. 30, 2018, Art. no. 064004.

[8] X. Wen *et al.*, "Doubly enhanced second harmonic generation through structural and epsilon-near-zero resonances in TiN nanostructures," *ACS Photon.*, vol. 5, no. 6, pp. 2087–2093, 2018.

[9] Y. B. Habibullah, K. Iwata, and T. Ishihara, "Second-harmonic generation from complementary au metasurfaces with triangular resonators," *J. Opt. Soc. Amer. B*, vol. 36, no. 4, pp. 1166–1175, 2019.

[10] C. K. Dass *et al.*, "Gap-plasmon-enhanced second-harmonic generation in epsilon-near-zero nanolayers," *ACS Photon.*, vol. 7, no. 1, pp. 174–179, 2020.

[11] D. J. Yang *et al.*, "Magnetic fano resonance-induced second-harmonic generation enhancement in plasmonic meta-molecule rings," *Nanoscale*, vol. 9, no. 18, pp. 6068–6075, 2017.

[12] G. D. Bernasconi, J. Butet, and O. J. F. Martin, "Dynamics of second-harmonic generation in a plasmonic silver nanorod," *ACS Photon.*, vol. 5, no. 8, pp. 3246–3254, 2018.

[13] B. Hazra, K. Das, and M. Chandra, "Large second harmonic generation from hollow gold nanoprisms: Role of plasmon hybridization and structural effects," *Phys. Chem. Chem. Phys.*, vol. 19, 2017, Art. no. 18394.

[14] K. Guo, Y. L. Zhang, C. Qian, and K. H. Fung, "Electric dipole-quadrupole hybridization induced enhancement of second-harmonic generation in T-shaped plasmonic heterodimers," *Opt. Exp.*, vol. 26, no. 9, pp. 11984–11993, 2018.

[15] K. Guo, C. Qian, Y. L. Zhang, and K. H. Fung, "Second harmonic generation manipulation enabled by electromagnetic coupling in bianisotropic metamolecules," *Adv. Opt. Mater.*, vol. 6, no. 7, 2018, Art. no. 1701154.

[16] A. Ahmadivand, B. Gerislioglu, R. Ahuja, and Y. K. Mishra, "Toroidal metaphotonics and metadevices," *Laser Photon. Rev.*, vol. 14, no. 11, 2020, Art. no. 1900326.

[17] N. Talebi, S. Guo, and P. A. van Aken, "Theory and applications of toroidal moments in electrodynamics: Their emergence, characteristics, and technological relevance," *Nanophotonics*, vol. 7, no. 1, pp. 93–110, 2018.

[18] T. Kaelberer, V. A. Fedotov, N. Papasimakis, D. P. Tsai, and N. I. Zheludev, "Toroidal dipolar response in a metamaterial," *Science*, vol. 330, pp. 1510–1512, 2010.

[19] K. Marinov, A. D. Boardman, V. A. Fedotov, and N. I. Zheludev, "Toroidal metamaterial," *New J. Phys.*, vol. 9, no. 9, 2007, Art. no. 324.

[20] Y. Fan, Z. Wei, H. Li, H. Chen, and C. M. Soukoulis, "Low-loss and high-Q planar metamaterial with toroidal moment," *Phys. Rev. B*, vol. 87, 2013, Art. no. 115417.

[21] A. C. Tasolamprou, O. Tsilipakos, M. Kafesaki, C. M. Soukoulis, and E. N. Economou, "Toroidal eigenmodes in all-dielectric metamolecules," *Phys. Rev. B*, vol. 94, 2016, Art. no. 205433.

[22] A. Ahmadivand and B. Gerislioglu, "Directional toroidal dipoles driven by oblique poloidal and loop current flows in plasmonic meta-atoms," *J. Phys. Chem. C*, vol. 122, no. 42, pp. 24304–24308, 2018.

[23] M. Gupta *et al.*, "Sharp toroidal resonances in planar terahertz metasurfaces," *Adv. Mater.*, vol. 28, pp. 8206–8211, 2016.

[24] A. Sayanskiy, M. Danaeifar, P. Kapitanova, and A. E. Miroshnichenko, "All-dielectric metalattice with enhanced toroidal dipole response," *Adv. Opt. Mater.*, vol. 6, no. 19, 2018, Art. no. 1800302.

[25] X. Cui. *et al.*, "Anapole states and toroidal resonances realized in simple gold nanoplate-on-mirror structures," *Adv. Opt. Mater.*, 2020, Art. no. 202001173.

[26] V. R. Tuz, V. V. Khardikov, and Y. S. Kivshar, "All-dielectric resonant metasurfaces with a strong toroidal response," *ACS Photon.*, vol. 5, no. 5, pp. 1871–1876, 2018.

[27] L. Liu *et al.*, "Toroidal dipolar response in plasmonic nanoparticle clusters," *J. Phys. D: Appl. Phys.*, vol. 51, no. 3, 2018, Art. no. 035106.

[28] R. C. Jin, J. Li, Y. H. Wang, M. J. Zhu, J. Q. Li, and Z. G. Dong, "Optical force enhancement and annular trapping by plasmonic toroidal resonance in a double-disk metastructure," *Opt. Exp.*, vol. 24, no. 24, pp. 27563–27568, 2016.

[29] M. Gupta, Y. K. Srivastava, M. Manjappa, and R. Singh, "Sensing with toroidal metamaterial," *Appl. Phys. Lett.*, vol. 110, no. 121108, 2017.

[30] J. Wang, N. Wang, J. Hu, and R. Jiang, "Toroidal dipole-induced absorption and scattering dip in (dielectric core)@(plasmonic shell) nanostructures," *Opt. Exp.*, vol. 25, no. 23, pp. 28935–28945, 2017.

[31] W. Liu, J. Zhang, and A. E. Miroshnichenko, "Toroidal dipole-induced transparency in core-shell nanoparticles," *Laser Photon. Rev.*, vol. 9, no. 5, pp. 564–570, 2015.

[32] L. Ge *et al.*, "Unidirectional scattering induced by the toroidal dipolar excitation in the system of plasmonic nanoparticles," *Opt. Exp.*, vol. 25, no. 10, pp. 10853–10862, 2017.

[33] A. Ahmadivand, M. Semmlinger, L. Dong, B. Gerislioglu, P. Nordlander, and N. J. Halas, "Toroidal dipole-enhanced third harmonic generation of deep ultraviolet light using plasmonic meta-atoms," *Nano Lett.*, vol. 19, no. 1, pp. 605–611, 2019.

[34] C. J. Tang, P. Zhan, Z. S. Cao, J. Pan, Z. Chen, and Z. L. Wang, "Magnetic field enhancement at optical frequencies through diffraction coupling of magnetic plasmon resonances in metamaterials," *Phys. Rev. B*, vol. 83, 2011, Art. no. 041402(R).

[35] C. Ciracì, E. Poutrina, M. Scalora, and D. R. Smith, "Second-harmonic generation in metallic nanoparticles: Clarification of the role of the surface," *Phys. Rev. B*, vol. 86, 2012, Art. no. 115451.

[36] M. Falasconi, L. C. Andreani, A. M. Malvezzi, M. Patrini, V. Mulloni, and L. Pavesi, "Bulk and surface contributions to second-order suscrptibility in crystalline and porous silicon by second-harmonic generation," *Surf. Sci.*, vol. 481, pp. 105–112, 2001.

[37] P. B. Johnson and R. W. Christy, "Optical constants of noble metals," *Phys. Rev. B*, vol. 6, no. 12, pp. 4370–4379, 1972.

[38] E. D. Palik, *Handbook of Optical Constants of Solids*, New York, NY, USA: Academic Press, 1985.